Metadata of the chapter that will be visualized in SpringerLink

Book Title	Nonlinear Dynamics for Biological Systems	
Series Title		
Chapter Title	The Dynamics of Sensorimotor Integration	
Copyright Year	2025	
Copyright HolderName	The Author(s), under exclusive license to Springer Nature Switzerland AG	
Author	Family Name	**Andrada** -> Carpio Andrada
	Particle	
	Given Name	**Agustín Carpio** -> Agustin
	Prefix	
	Suffix	
	Role	
	Division	Departamento de Física, Facultad de Ciencias Exactas y Naturales
	Organization	Ciudad Universitaria, Universidad de Buenos Aires
	Address	Buenos Aires, Argentina
	Division	
	Organization	Instituto de Física Interdisciplinaria y Aplicada (INFINA), Ciudad Universitaria, CONICET - Universidad de Buenos Aires
	Address	Buenos Aires, Argentina
	Email	aguscarpio@gmail.com
Corresponding Author	Family Name	**Mindlin**
	Particle	
	Given Name	**Gabriel B.**
	Prefix	
	Suffix	
	Role	
	Division	Departamento de Física, Facultad de Ciencias Exactas y Naturales
	Organization	Ciudad Universitaria, Universidad de Buenos Aires
	Address	Buenos Aires, Argentina
	Division	
	Organization	Instituto de Física Interdisciplinaria y Aplicada (INFINA), Ciudad Universitaria, CONICET - Universidad de Buenos Aires
	Address	Buenos Aires, Argentina
	Email	gabo@df.uba.ar

Abstract

Sensorimotor integration refers to how the sensory feedback originating from motor actions influences the generation of motor patterns. From a dynamic perspective, this can be understood as the impact of a term in the equations governing motor behavior, which is dependent on the variables of the problem in previous instances. An important motor pattern is the generation of periodic behavior, and in this work, we will discuss the impact of delayed feedback in a system capable of displaying these patterns. This question has been addressed when the appearance of periodic motor patterns is due to a Hopf bifurcation. Here we review those results, and then move to explore the rich emergent dynamics arising in delayed systems near a Saddle-Node In Limit Cycle (SNILC) bifurcation. Our results reveal a complex subharmonic structure consistent with known activity patterns in multiple fields. We also explore potential applications of this dynamic phenomenon.

The Dynamics of Sensorimotor Integration

Agustín Carpio Andrada and Gabriel B. Mindlin

Abstract Sensorimotor integration refers to how the sensory feedback originating from motor actions influences the generation of motor patterns. From a dynamic perspective, this can be understood as the impact of a term in the equations governing motor behavior, which is dependent on the variables of the problem in previous instances. An important motor pattern is the generation of periodic behavior, and in this work, we will discuss the impact of delayed feedback in a system capable of displaying these patterns. This question has been addressed when the appearance of periodic motor patterns is due to a Hopf bifurcation. Here we review those results, and then move to explore the rich emergent dynamics arising in delayed systems near a Saddle-Node In Limit Cycle (SNILC) bifurcation. Our results reveal a complex subharmonic structure consistent with known activity patterns in multiple fields. We also explore potential applications of this dynamic phenomenon.

AQ1

1 Introduction

Over the past few decades, extensive research has been conducted to comprehend the neural control of movement. By employing straightforward computational models to depict the actions of a single neuron or the collective actions of a neural population, it became feasible to construct basic networks capable of generating a diverse range of spatio-temporal patterns. These can be interpreted as the physiological instructions controlling the biomechanics of some peripheral system.

Certain networks, characterized as dynamical systems, exhibit the ability to yield diverse solutions contingent on specific global parameters. This capability has proven instrumental in shedding light on various phenomena, notably contributing to our

A. C. Andrada · G. B. Mindlin (✉) A. C. Andrada -> A. Carpio Andrada
Departamento de Física, Facultad de Ciencias Exactas y Naturales, Ciudad Universitaria, Universidad de Buenos Aires, Buenos Aires, Argentina
e-mail: gabo@df.uba.ar

Instituto de Física Interdisciplinaria y Aplicada (INFINA), Ciudad Universitaria, CONICET - Universidad de Buenos Aires, Buenos Aires, Argentina

M. Stich and J. Carballido-Landeira (eds.), *Nonlinear Dynamics for Biological Systems*, SEMA SIMAI Springer Series 40,
https://doi.org/10.1007/978-3-031-99044-1_1

understanding of distinct gaits observed in locomotion. In the 1970s, physiologists drew inspiration from engineering control systems to gain insight into processes involving feedback, thereby enhancing the comprehensive description of behavior.

The behavior of an animal, for instance when it is executing a motor plan, emerges from the intricate interplay among its nervous system, its motor morphological structures, and the sensory information gathered from its environment. This interaction operates bidirectionally, as the environment is also influenced by the animal's behavior. The concept of "sensory feedback" encompasses the mechanism through which animals perceive and assess the consequences of their actions on the environment. In parallel, "sensorimotor integration" involves the process by which motor output, or behavior in general, materializes through the interplay between two information channels: sensory input processing and motor plan pathways [21].

The research program is simple to articulate, yet its implementation is not without challenges, primarily due to the intricacies involved in deciphering the coding of sensory information. Within the framework of functionalism in neuroscience, the nervous system processes sensory input based on its intended purpose and destination. When the goal is perception, the processing may entail feature extraction and the amalgamation of inputs from various sensory sources. Conversely, if the sensory input is employed to guide the generation of motor commands, it must be interpreted in relation to the present state of the motor system and how it may change the course of execution of motor plans.

Repetitive sequencing of actions is a prevalent phenomenon in behavioral sequences, particularly observed in animal vocalizations. Notably, many species of birds construct their songs through the iterative repetition of specific syllables, followed by a sequence featuring a distinct syllable. Elementary models elucidating birdsong production reveal that these reiterated syllables can be produced through periodic physiological instructions governing respiration and the configuration of the vocal organ. The generation of different syllables can be achieved by modifying the relative phases of these instructions or other features such as their periods.

Extensive research has been dedicated to the avian song system, with a consensus emerging that a specific brain area within the telencephalon, known as HVC (proper name, formerly stood for high vocal center), plays a pivotal role in temporal pattern generation. Moreover, it is established that the auditory pathway projects into this brain region. Consequently, it is reasonable to inquire whether auditory feedback plays a crucial role in sustaining syllable repetitions in certain bird species. Corroborating this hypothesis, experiments with Bengalese finches indicate that deafening leads to a reduction in syllable repetitions. For the case of birdsong, the study of a computational model showed that syllable repeats are initially sustained by auditory feedback [21]. However, periodic patterns of activity are pervasive in nature and manifest in a variety of animal behaviors [20, 22]. The hypothesis posits that, in certain contexts, rhythmic activity emerges from the collective behavior of neural oscillators, which generate periodic signals driving the animal's motor systems [11].

A neural oscillator, a simple neural architecture capable of instigating periodic activity within the brain, comprises a pair of interconnected excitatory and inhibitory neurons [7]. When a local population of neurons exhibits comparable dynamics and

functionality, extending the neural oscillator model from a pair of neurons to a pair of populations using mean field theory becomes advantageous [9, 16]. The comprehension of these oscillators' dynamics and their interaction with other components of the nervous system, such as those conveying sensory feedback, is crucial for unraveling the mechanisms underpinning the generation of periodic behavior. Mathematically, this endeavor necessitates a thorough review of the impact of incorporating a delayed function of the variables used to describe the problem in the model elucidating the origin of the oscillations.

This issue has been previously investigated in [15], where the impact of delayed feedback on a basic oscillator is explored. This seminal work modeled the oscillator as the normal form of a Hopf bifurcation, which is a simple representation of how oscillations arise in nonlinear systems. In a Hopf bifurcation, oscillations emerge with zero amplitude and a distinct frequency. Building upon this foundation, our study extends the previous research by examining the effects of delayed feedback in proximity to global bifurcations. Furthermore, we investigate this problem within the framework of an interpretable model for neural oscillators.

In computational neuroscience, the Wilson-Cowan model [19] delineates the dynamics governing interactions among populations of elementary excitatory and inhibitory model neurons. Originating from the collaborative work of Hugh R. Wilson and Jack D. Cowan, this model has found widespread application in neuronal population modeling, with various adaptations gaining prominence. Notably, the model holds historical significance for its utilization of phase plane methods and numerical solutions to elucidate the responses of neuronal populations to stimuli.

A distinctive feature of the Wilson-Cowan model is its depiction of the interplay between a population that stimulates the neurons it connects to and a population that inhibits its efferents (the neurons it connects to). As a consequence of this interaction, a common dynamical outcome is the emergence of oscillations. Oscillations within a Wilson-Cowan model can emerge not only through local bifurcations like Hopf bifurcations but also through global bifurcations, exemplified by the Saddle-Node In Limit Cycle bifurcation (SNILC). In this type of bifurcation, a local Saddle-Node bifurcation takes place, but since the unstable manifold of the saddle is part of the stable manifold of the attractor, the disappearance of the fixed points gives rise to a periodic solution with infinite period at the bifurcation (for this reason, SNIPER is an alternative name for this bifurcation; it stands for Saddle Node in Infinite Period). Notice that the values of the vector field in the region of the phase space where the two fixed points collapsed will be close to zero. Therefore, the periodic trajectory will be slow (critical slowing down phenomena) in that region of the phase space. Consequently, the oscillations exhibit a composite structure, comprising both fast and slow components. This distinctive feature sets them apart from simple harmonic oscillations. Another consequence is that the periodic solutions being born in these bifurcations contain a rich spectral content.

These bifurcation types are closely related to neuronal excitability classes, such as Type I and Type II, as described in [12]

The richness of the dynamics in the Wilson-Cowan oscillator suggests that to comprehend the integration of a sensorimotor effect, translated mathematically through the inclusion of a delay term, one must delve beyond the impact of such terms on a simple Hopf oscillator. For this reason, in this chapter, we will scrutinize the

605223_1_En_1_Chapter-online ☑ TYPESET ☐ DISK ☐ LE ☑ CP Disp.:8/8/2025 Pages: 15 Layout: T1-Standard

bifurcations inherent in the dynamics of a Wilson-Cowan oscillator and explore the repercussions of introducing delayed terms to the model when it is close to a SNILC bifurcation. By incorporating these delays, our goal is to delve into the potential dynamics that emerge when the onset of periodic motor control integrates with sensory feedback. The inclusion of delay in this context signifies the cumulative time required for motor behavior to undergo sensory integration and subsequently feed back into the motor program.

This chapter is structured as follows: Sect. 2 revisits a study conducted by Ramana Reddy et al. [15] that investigates the effects of time-delayed linear and nonlinear feedback on the dynamics of a single Hopf bifurcation oscillator. In Sect. 3, we present a comprehensive analysis of the proposed model, including a phase plane analysis that examines various dynamical regimes. Furthermore, we provide a complete bifurcation map of the system when the delayed term is omitted. Section 4 explores the influence of delayed feedback on the model. We construct a map that illustrates the range of periodic solutions in a delay-parameter space (a $K \times \tau$ space where K represents the amplitude of a delayed feedback and τ its delay-time lag). Our findings reveal increased complexity due to the introduction of a delay-term exhibiting period-doubling bifurcations, hysteresis, and phase-locking to a spectrum of subharmonic solutions. Finally, Sect. 5 summarizes the key findings and implications of our study. Additionally, we discuss future research directions, including a biological perspective on oscillatory neural activity and periodic patterns observed in animal behavior.

2 The Effect of Feedback on Systems Close to Hopf and Saddle-Node-in-Limit-Cycle Bifurcations

Normal forms are the simplest equations consistent with a linear singularity, where simple refers to the minimal number of monomial terms in the vector field up to a given order. For the case of a Hopf bifurcation, the qualitative change in the flow being the birth of a limit cycle of zero amplitude and finite frequency, the normal form for a complex variable depending on time $Z(t)$ reads as follows:

$$\dot{Z}(t) = (a + i\omega - |Z(t)|^2)Z(t), \tag{1}$$

where a is a real constant and ω denotes the frequency at which oscillations arise in the absence of feedback. For its simplicity, it serves as a widely utilized dynamical system for representing periodic behavior. In [15], the authors introduce a feedback term to the system as follows:

$$\dot{Z}(t) = (a + i\omega - |Z(t)|^2)Z(t) - KZ(t - \tau), \tag{2}$$

where K represents the amplification factor of the delayed term, and τ corresponds to the time delay. The delayed feedback term, $KZ(t-\tau)$, accounts for the contribution of the system's activity at time $t-\tau$ to its behavior at time t, weighted by the factor K. When $K=0$, the system exhibits a stable limit cycle with an amplitude of $\sqrt{a}$ and an angular frequency of ω.

By expressing the system in polar coordinates and setting $a=1$, we can rewrite the equations as:

$$\dot{r}(t) = [1 - r^2(t)]r(t) - Kr(t-\tau)\cos[\theta(t-\tau) - \theta(t)] \tag{3}$$

$$\dot{\theta}(t) = \omega - K\frac{r(t-\tau)}{r(t)}\sin[\theta(t-\tau) - \theta(t)]. \tag{4}$$

Considering solutions of the form $Z(t) = Re^{i\Omega t}$ for $\tau > 0$, we anticipate solutions in polar form as $r(t) = R$ and $\theta(t) = \Omega t$, where R and Ω are real constants. Thus, we can deduce the mathematical conditions for the amplitude and frequency of the oscillator in the periodic solution:

$$R = \sqrt{1 - K\cos(\Omega\tau)} \tag{5}$$

$$\Omega = \omega + K\sin(\Omega\tau) \tag{6}$$

Graphically, Eq. (6) reveals that the frequencies of the solutions correspond to the intersection points of the identity function $f(\Omega) = \Omega$ and $g(\Omega) = \omega + K\sin(\Omega\tau)$. Under specific conditions of ω and τ, multiple intersections exist, indicating the presence of multiple periodic solutions. An example demonstrating this phenomenon is illustrated in Fig. 1.

Indeed, the inclusion of feedback imposes a significant constraint on the frequencies at which periodic oscillations can exist. This is in stark contrast to the situation without feedback, where a limit cycle can exist for any value of Ω. The introduction of delayed feedback introduces a condition that restricts the possible frequencies at which sustained oscillations can occur. This constraint arises from the interplay between the intrinsic frequency of the system, represented by ω, and the influence of the delayed feedback term. As a result, the system's dynamics exhibits a more intricate behavior, characterized by a limited range of frequencies that support sustained oscillations.

In situations where multiple stable solutions coexist for a given parameter set, the system's evolution towards a specific stable solution depends on the initial condition. These initial condition can be conceptualized as a vector with infinitely many complex elements, representing the system's states for every t between $-\tau$ and 0 (if we start integrating from $t=0$).

Numerical simulations have confirmed the presence of hysteresis phenomena (dependence of the state of a system on its history) associated with the existence of multiple stable periodic solutions. Depending on the initial condition, the system may converge towards one particular stable solution or another, leading to distinct

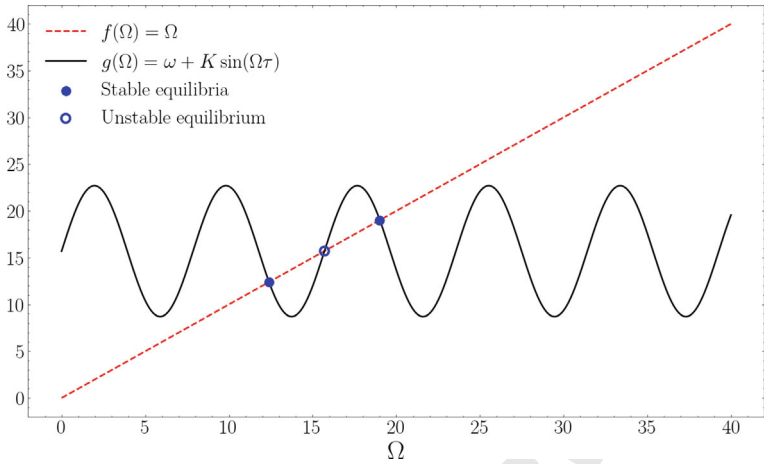

Fig. 1 Periods of rhythmic solutions in Eq. (1) are given by the intersection of $f(\Omega)$ and $g(\Omega)$. In this example, two stable and one unstable solutions exists with parameters $\omega = 15.7$, $K = 7$, $\tau = 0.8$

exists -> exist

dynamical behaviors and trajectories. This behavior highlights the sensitivity of the system to its initial state and the rich complexity arising from the coexistence of multiple stable solutions.

The study of under which conditions a system's vector field undergoes a topological change can be addressed by bifurcation theory. For a two-dimensional dynamical system described by its associated Jacobian matrix (the matrix of all the system's first-order partial derivatives), specific conditions determine the occurrence of the Saddle-Node and Hopf bifurcations. The Saddle-Node bifurcation condition is given by $D = 0$, where D represents the determinant of the Jacobian matrix. When $D = 0$, a Saddle-Node bifurcation occurs, resulting in the creation or destruction of a pair of equilibrium points.

On the other hand, the Hopf bifurcation condition is satisfied when $T = 0$ and $D > 0$, leading to the birth or annihilation of a limit cycle, where T stands for the trace of the Jacobian matrix. These conditions provide insights into the behavior and qualitative changes that occur in the system as its parameters are varied, helping to understand the occurrence of bifurcations and the emergence of different dynamical regimes.

Unlike the Hopf bifurcation, which typically gives rise to periodic solutions with a well defined finite frequency, the SNILC bifurcation exhibits a distinct behavior characterized by the emergence of periodic solutions which are born with infinite period. This results in a diverse set of periodic behaviors that span a broad range of time scales [4] for parameters in the vicinity of the bifurcation. This wide range of periods adds richness and complexity to the system dynamics, offering a broader repertoire of possible behaviors compared to other bifurcations.

Notice that the SNILC bifurcation is global in nature. Hence, we will explore the effect of feedback on a simple and pertinent system of equations that, with minimal complexity, is able to describe neural oscillations born in SNILC bifurcations.

Now that we know some of the features that usually emerge in delayed feedback systems, let's take a step back to gently introduce the Wilson-Cowan neural oscillator model. In Sect. 3 we present the system and describe it in terms of bifurcation theory for the ordinary form (i.e. with the delay term multiplied by zero). Then in Sect. 4, we explore in depth the effects of a delayed copy of the system's activity feeding back into itself while varying the delay related parameters. The use of this set of equations allows a smooth export to the realm of neuroscience, where sensorimotor integration of major importance.

3 The Dynamics of Neural Oscillators

We start reviewing the solutions of a Wilson-Cowan oscillator, which is a system designed to describe the dynamics of two interacting populations of neurons: excitatory and inhibitory. Our goal is to modify the model in order to incorporate the effect of feedback, which can be interpreted as the sensory processing of changes resulting from the system's own activity (i.e., sensory feedback). To achieve this, we introduce a delayed copy of one of the variables as an input to the system:

$$\begin{cases} \dot{x} &= \mu(-x + S(\rho_x + ax - by)) \\ \dot{y} &= \mu(-y + S(\rho_y + cx - dy + Kx(t-\tau)) \end{cases}. \quad (7)$$

The state variables $x = x(t)$ and $y = y(t)$ represent the excitatory and inhibitory neural activities, respectively. The parameter μ governs the intrinsic time scale of the population's average firing rate. The sigmoid function $S(x) = \frac{1}{1+e^{-x}}$ captures the processing of inputs from both populations, weighted by synaptic strength coefficients a, b, c, and d, as well as external stimuli ρ_x and ρ_y. The time-delayed copy of the excitatory activity $x(t-\tau)$, serves as an input to the inhibitory population at time t. This accounts for the feedback effect on the neural dynamics in our model. This delayed input is multiplied by a factor K, representing an amplification factor. Note that the linear copy $x(t-\tau)$ is the simplest way to introduce delayed feedback into the system. Figure 2 provides a graphical representation of the described model.

Consider $K = 0$ (the ordinary non-delayed version of the system). In this case, Eq. (7) simply reduces to:

$$\begin{cases} \dot{x} &= \mu(-x + S(\rho_x + ax - by)) \\ \dot{y} &= \mu(-y + S(\rho_y + cx - dy)) \end{cases}. \quad (8)$$

This dynamical system serves as a model for the emergence of periodic patterns in the absence of sensory feedback. The condition for equilibrium is given by both

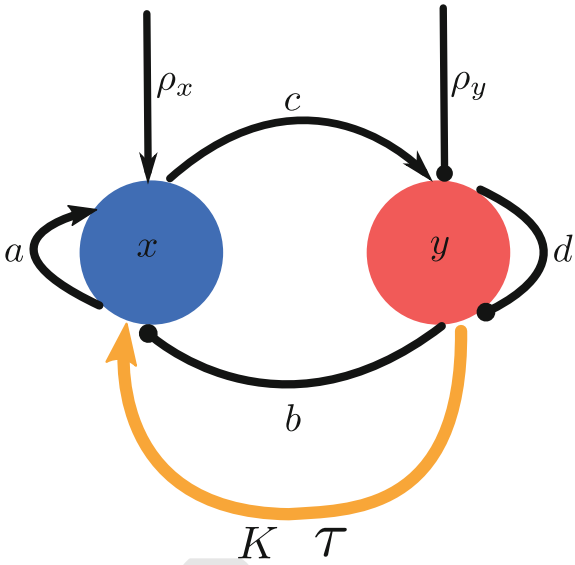

Fig. 2 Illustration of the delayed Wilson-Cowan model depicting excitatory (blue circle) and inhibitory (red circle) populations of neurons, and their activities denoted by x and y respectively. The synaptic parameters of the model, denoted by a, b, c, and d, as well as the input parameters ρ_x and ρ_y, are shown. Additionally, the delay-related parameters K and τ are indicated

derivatives being equal to zero. So, a fixed point defined as $P^* = (x^*, y^*)$ must satisfy the condition:

$$\begin{cases} x^* &= S(\rho_x + ax - by) \\ y^* &= S(\rho_y + cx - dy) \end{cases}. \tag{9}$$

Therefore, the Jacobian matrix corresponding to Eq. (8), denoted by J, which evaluated at the fixed points reads as:

$$J = \begin{bmatrix} -1 + aS'(\rho_x + ax - by) & -bS'(\rho_x + ax - by) \\ cS'(\rho_y + cx - dy) & -1 - dS'(\rho_y + cx - dy) \end{bmatrix}. \tag{10}$$

J can be expressed in a more convenient form as shown, addressing the fact that the derivative of the sigmoid function, S', is equal to $S(1 - S)$ (full details on [7]):

$$J = \begin{bmatrix} -1 + ax(1 - x) & -bx(1 - x) \\ cy(1 - y) & -1 - dy(1 - y) \end{bmatrix}. \tag{11}$$

The Saddle-Node bifurcation occurs when the determinant of the evaluated Jacobian matrix becomes zero. However, the impact of this bifurcation on the system depends on factors beyond the mere change in sign of the determinant.

The occurrence of a Saddle-Node bifurcation does not necessarily imply the creation or destruction of a limit cycle. Determining whether a limit cycle is formed or destroyed as a result of the bifurcation depends on a comprehensive analysis of the system's global behavior, taking into account other components and factors. This

particular case of Saddle-Node bifurcation is referred to as Saddle-Node in Limit Cycle bifurcation (SNILC).

In this section we describe the bifurcation diagram (a plot where multiple bifurcation curves are depicted in a parameter space, in this case the $\rho_x \times \rho_y$ space) of the model for the case of $K = 0$ and specific parameter values ($a = b = c = 10$, $d = -10$). These particular parameter values are selected to ensure that the boundaries of the oscillatory regime in the parameter space correspond to SNILC bifurcation curves and none of them to Hopf bifurcations.

Phase portraits provide a concise graphical representation of the qualitative behavior of the solutions of a system under specific parameter values [17]. When the system undergoes a bifurcation as a result of a change of parameters, the corresponding phase portraits exhibit distinct qualitative characteristics.

In our analysis, we will focus on the following features depicted in the phase portraits:

- The positions of fixed points
- The presence of closed orbits or limit cycles
- Trajectories of the system, which provide insights into the stability of fixed points and the direction of flow within the system.

As shown in Fig. 3, the central region of the parameter space displays distinctive periodic behavior characterized by limit cycle dynamics. This region is enclosed by SNILC bifurcation curves. In the proximity of the bifurcation, the period of a solution gradually increases as we approach the bifurcation point. Upon crossing the SNILC bifurcation, the system transitions into a quiescent regime, where sustained oscillations cease to exist.

Phase portraits were obtained by numerically integrating the system and analytically finding the fixed points. A representative phase portrait that captures the qualitative dynamics is drawn for each of the relevant parameter space regions delimited by bifurcation curves given by the parameters of that region. To provide a comprehensive understanding of the various dynamic regimes, we conducted an exploration along both local and global bifurcation curves.

In Fig. 3 we show both the local bifurcation curves and the global ones (including the homoclinic bifurcation curve depicted in blue). It is worth mentioning that some of the black curves depicting Saddle-Node bifurcations also correspond to global bifurcations, since some of them are SNILC.

So far, we have focused on the qualitative differences observed in the system's dynamics, evaluated in different regions of the $\rho_x \times \rho_y$ parameter space. However, it is important to note that in the vicinity of a bifurcation leading to qualitative changes, there exists a spectrum of quantitatively distinct solutions. Specifically, when the system is close to a SNILC bifurcation and a simple limit cycle is present, the periods of the solutions span a wide range even with small variations in the parameters. This is illustrated in Fig. 4, where we observe the variation in periods for different parameter values.

Having completed a comprehensive qualitative analysis of the dynamic regimes in the system, we are now poised to delve into the investigation of the effects of

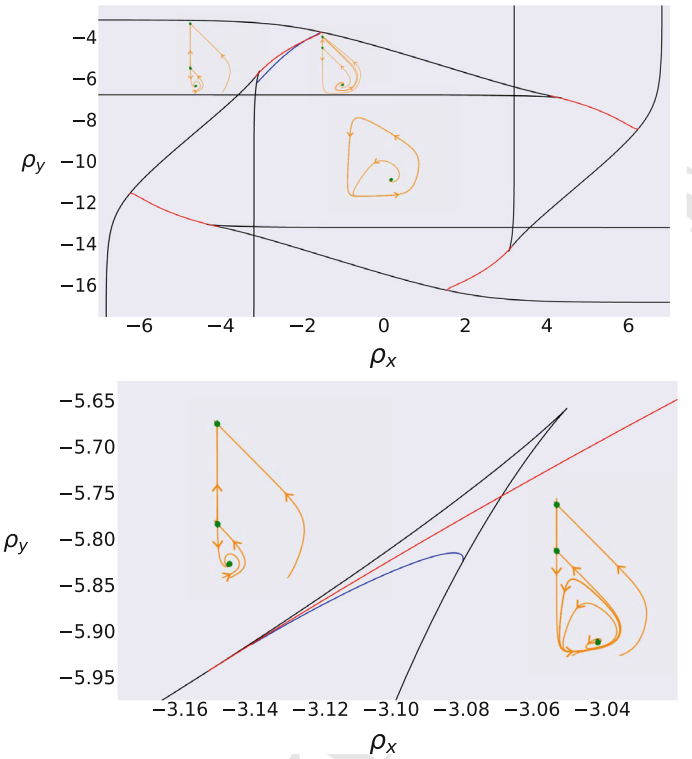

Fig. 3 Wilson-Cowan bifurcation map. Lower panel is a zoom of the top panel. The Saddle-Node bifurcation curves are represented in black, the Hopf bifurcation curves in red and the Homoclinic bifurcation curves in blue. Phase portraits (in orange) corresponding to the different delimited regions are represented inside the regions. Qualitatively equal phase portraits (as consequence of symmetry) and those with 5 fixed points were omitted. It should be noted that, for simplicity, neither the node-spiral transitions nor the double limit cycle bifurcation has been represented in the map. Likewise, the parts of the Saddle-Node bifurcation that are also SNILC have not been distinguished, nor have the subcritical and supercritical parts of the Hopf bifurcation

-> "as a consequence"

delayed feedback. By incorporating this additional factor into the problem, we aim to gain insights into how it influences the system's behavior. This next section will explore the intriguing interplay between delayed feedback and the existing dynamic regimes, shedding light on the complex dynamics that emerge from this interaction.

4 The Effect of Feedback on Neural Oscillators

In this section, we introduce feedback into the neural oscillator model, following a similar approach as in previous studies [13–15]. By incorporating a non-zero value for the feedback parameter K in Eq. (7), the system becomes sensitive to its own

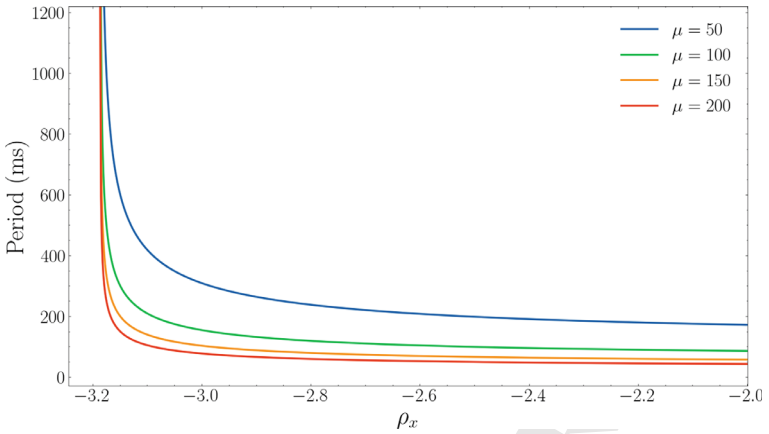

Fig. 4 Period against ρ_x for multiple values of μ in Eq. (7) with $a = b = c = 10$, $d = -10$, $\rho_y = -9$ and $K = 0$. Note that solutions' periods tend to infinity when ρ_x tends to the critical value for the SNILC bifurcation $\rho_x' \approx -3.2$

past states. To capture this effect computationally, we employ a queue-like structure to store the system states from $t - \tau$ to t, where τ represents the time delay. This structure is updated at each step of the numerical integration, which is performed using a fourth-order delay-adapted Runge-Kutta method. Additionally, we include an option to consider the state vector from the immediately previous computation in consecutive simulations, providing continuity in the analysis.

For the subsequent analysis, we will fix the non-delay parameters of Eq. (7) as described in the caption of Fig. 5, which guarantees the proximity to a SNILC. We then proceeded to explore the dynamics as K and τ are varied.

In the absence of feedback ($K = 0$), the system exhibits periodic solutions with a period duration of 65 ms. To explore the effects of feedback, we employed the modified fourth-order Runge-Kutta method discussed earlier to numerically compute the trajectories of the system. By integrating the equations over a wide range of K and τ values, we obtained the corresponding trajectories and investigated their characteristics. To comprehensively analyze the impact of feedback, we explored a subset of the $K \times \tau$ parameter space, where K ranges from 3 to 10 and τ ranges from 40 to 70 ms. By doing so, we aim to uncover the emerging complexity in the delayed version of the model.

The incorporation of a delay allows us to retain and analyze the previous states of the system in a "queue" structure. With this capability, we can traverse the $K \times \tau$ space in all four directions (ascending and descending values of K and τ, while keeping the other parameter constant) and investigate how these variations lead to the generation of qualitatively and/or quantitatively different periodic solutions. By examining the trajectories obtained for each K and τ combination, we can gain insights into the nature and diversity of the system's dynamics.

It is worth noting that the analysis of the solutions is performed disregarding any transients that may appear when increasing or decreasing a parameter between consecutive integrations. Since the length of the initial condition vector grows for consecutive integrations when τ is increasing, the stored states of the system must be long enough to avoid running short of stored values for $x(t-\tau)$ and $y(t-\tau)$.

At each point in the parameter space grid, we applied an algorithm to calculate the periodicity of the solution. This algorithm involved tracking the number of rotations in the trajectory until it repeated itself, with a predefined threshold for the difference between $f(t)$ and $f(t+T)$ for multiple values of t, where T represented a candidate period duration. To be precise, the algorithm consists in the following steps and can be implemented in the desired programming language:

- A variable *rotationCounter* is initialized. At each point in the phase plane it grows by the value corresponding to the angular velocity measured over the vector field divided by 2π.
- For a given (x, y) time series (a trajectory), we obtain a time series for *rotationCounter*. Every integer *rotationCounter* (up to the desired maximum periodicity, in our case 8) in the time series becomes a candidate to be the n of the n-periodicity of the solution. T is the candidate period duration associated to that *rotationCounter*.
- Each of the *rotationCounter* candidates gets a score proportional to the average of the distances of $(x(t), y(t))$ and $(x(t+T), y(t+T))$ for s representative amount of times t.
- The minimum *rotationCounter* whose score is less than a fixed threshold is considered the n-period of the solution. That's the output of the algorithm.
- If no integer *rotationCounter* gets a score below the threshold, the algorithm outputs *null*.
- Precision can be increased by increasing the number of evaluated points in time to compute the distances and/or decreasing the threshold (it must be taken into account that decreasing too much the threshold without increasing accordingly the numerical precision of the integrator could produce undesired *null* outputs).

It must be noted that the classification is purely topological and not temporal. This means, for instance, that n-periodic solutions might have very different time periods for the same n. It also means that, for example, a 2-periodic solution may correspond to a longer time period than a 3-periodic one.

To visually represent our findings, we assigned integer values to classify the periodicity of the solutions at each explored grid coordinate of the parameter space. We used a color-coding scheme where unique colors were assigned to integer values up to 8. By superimposing the resulting areas from the four plots with transparency, we created a composite visualization shown in Fig. 5. White regions indicate cases where no periodicity was detected by the algorithm. These regions may correspond to higher period, quasiperiodic or chaotic solutions.

This approach allows us to gain insight into the presence and characteristics of periodic solutions across the $K \times \tau$ parameter space, providing a comprehensive view of the system's harmonic structure that emerges as a consequence of the applied

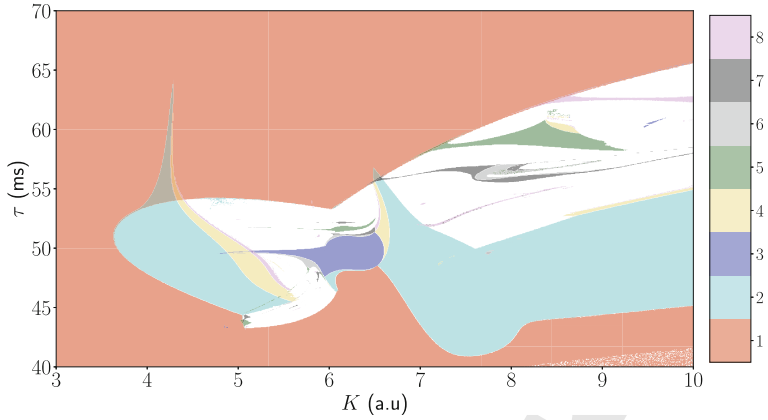

Fig. 5 Harmonic bifurcation map in delay-parameters space ($K \times \tau$) with $\rho_x = -2.3$, $\rho_y = -9$ and $\mu = 150$. Each colored region is linked to a periodic solution of n-periodicity, being n an integer between 1 and 8. Transparency enables a way to visualize bistable zones since the plot was constructed by merging the areas of n-periodicity obtained by determining the period of the solutions of the system when integrated for the $K \times \tau$ parameter space explored in the four directions (increasing or decreasing each delay-related parameter). A rich spectrum of subharmonic solutions is observed. Uncolored regions are those where the solution was not n-periodic for any $n \leq 8$, i.e. higher periods, quasiperiodic or chaotic solutions

with n being an integer

feedback. We observe a rich subharmonic structure, meaning that the periods of the oscillatory solutions of the system are integer multiples of a fundamental. Values below $K = 3$ and $\tau = 40$ ms are omitted in the plot because there are only period-1 solutions.

Figure 5 displays the regions where specific periodic solutions occur and where pairs of different n-periodic stable solutions coexist (so transparency allows to identify bistable regions as those with two colors). The color-coded map enables the identification of adjacent zones and their colors, allowing us to discern the permitted transitions between periodic solutions and their locations. This plot bears resemblance to Arnold's tongues observed in the study of the circle map [2].

The presence of multistability, where multiple periodic stable solutions coexist for certain parameter combinations, is a prominent feature observed in our results. This finding is consistent with previous research conducted on oscillator systems with time delay [8]. The identification and characterization of multistability adds to our understanding of the complex dynamics exhibited by the delayed version of the model.

The observed increase in complexity and the emergence of rich solutions in our model can be attributed solely to the introduction of a simple delay term, represented by a linear copy of the value of x at a past time $t - \tau$. No other modifications were made to the model. This highlights the profound impact of delayed feedback on the dynamics of the system.

Since pairs of adjacent areas in which one doubles the periodicity of the other are extensively well represented in Fig. 5, we may state that the presence of period-doubling bifurcations is a remarkable emergent feature of the system.

To further explore the effects of delay, it would be interesting for future investigations to consider the influence of nonlinear delayed terms. Nonlinearities in the delay term can introduce additional complexities and potentially lead to even richer dynamics.

It is important to note that the inclusion of a delay term deviates from the principles of traditional dynamical systems theory, where a finite set of initial conditions determines the unique fate of the system. In the case of a differential equation with delays, the problem becomes infinite-dimensional, as it requires a continuous range of states as initial condition to integrate the equations accurately. This departure from finite-dimensional dynamics adds another layer of complexity to the analysis and understanding of the system's behavior.

5 Discussion

The Wilson-Cowan model is widely recognized as a valuable tool for investigating the dynamics of neural populations. To gain a comprehensive understanding of this model, it is crucial to examine its behavior under various conditions. In this study, we specifically delved into the influence of time-delayed feedback on the dynamics of the Wilson-Cowan oscillator model. Our primary focus was on the emergence of a subharmonic structure in close proximity to a SNILC bifurcation. By exploring this aspect, we aimed to shed light on the intricate relationship between delayed feedback and the complex dynamics observed in neural systems.

The inclusion of the simplest feedback term in the Wilson-Cowan model revealed a complex subharmonic structure. It has been shown that multiple stable solutions exists for some parameter values. To which of the stable solutions the system locks is highly dependent of the previous states (and so, of the direction in which the parameter space is explored). This is a signature of hysteresis because the state of the system is dependent on its history: for two different vectors representing the states of the system between times $t - \tau$ and t, qualitatively different solutions may arise for exactly the same set of parameters.

In sensory physiology, phase locking refers to the firing of neurons preferentially at a certain phase of an amplitude-modulated stimulus. The neural oscillator we are modelling is one in which a linear delayed copy of the activity acts as a stimulus feeding back the system. The delay-time may be understood as the phase of a driving force to which the activity may synchronize either in a 1:1 way or as a subharmonic.

The implications of our findings extend beyond the realm of neuroscience and can be valuable in diverse fields such as physics and robotics. The complex dynamics observed in this model open up new possibilities for modeling and understanding intricate systems in various domains.

As a well-defined subharmonic structure is a characteristic pattern observed in the behavior of many biological systems, our results hold significant implications for both modeling and understanding the underlying mechanisms of these systems. By shedding light on the complex dynamics of the Wilson-Cowan model, our study may contribute to a better understanding of the behavior of biological systems and the potential applications of such models. Experiments to test the predictions could provide insights to the mechanisms that are actually involved in the production of periodical patterns with such characteristics.

Many animal behaviors are repeated multiple times over a relatively short period of time. It is likely that such repetitive actions are generated by oscillatory patterns of neural activity. In particular, birdsong is an animal model which is worth exploring under this perspective and has numerous parallels with human speech [3]. In many species, as canaries, the generation of the song involves the generation of periodic gestures, both respiratory and syringeal [10, 18]. The timing of these gestures is believed to be encoded in the HVC telencephalic nucleus. Research has provided evidence of glutamatergic and GABAergic synapses within the HVC, suggesting their involvement in the timing mechanisms of birdsong generation [11].

It is also known that HVC works as a relay center for both motor and auditory signals in the production and perception of birdsong [1]. It generates motor commands involved in song generation. Simultaneously, the HVC integrates auditory feedback by processing the auditory signals resulting from the bird's own vocalizations. The relevance of this mechanism varies depending on the degree of development of the HVC nucleus and the specific characteristics of each species.

Given the complex nature of birdsong and the involvement of motor and auditory systems, it is reasonable to speculate that some degree of processing delay exists. This delay can arise from various factors, including the time required for the song to be generated, propagated, and processed by the auditory system [5]. Studies have suggested that such delays may be involved in feedback mechanisms that regulate and fine-tune the production of birdsong [5].

Understanding the role of delayed feedback in the neural dynamics of birdsong can provide insights into how temporal processing and integration contribute to the generation and perception of complex vocalizations. Further experiments would be necessary to investigate the potential role of the sub-harmonic generation mechanisms described here in relation to the observed time durations of different syllable gestures. -> "subharmonic"

In conclusion, this model not only holds significance within the realm of the neuroscience of vocal learning but also unveils a broader perspective on sensorimotor integration, a fundamental mechanism that resonates across diverse challenges in animal behavior. Our exploration into the modeling of this phenomenon, particularly in the context of two pivotal bifurcations, Hopf and SNILC, serves as a gateway to understanding a spectrum of periodic patterns. By establishing itself as a template, this study opens the door to a comprehensive investigation into sensorimotor integration, transcending specific examples and offering a lens through which the intricacies of this fundamental process can be unravelled in a more universal context. AQ2

References

1. Amador, A., Margoliash, D.: Auditory Memories and Feedback Processing for Vocal Learning, pp. 561–575. (2010)
2. Arnold, V.I.: Small denominators. I. Mapping the circle onto itself. Izv. Akad. Nauk SSSR Ser. Mat. **25**, 21–86 (1961)
3. Doupe, A.J., Kuhl, P.K.: Birdsong and human speech: common themes and mechanisms. Annu. Rev. Neurosci. **22**(1), 567–631 (1999)
4. Ermentrout, G.B., Kopell, N.: Parabolic bursting in an excitable system coupled with a slow oscillation. SIAM J. Appl. Math. **46**(2), 233–253 (1986)
5. Fukushima, M., Margoliash, D.: The effects of delayed auditory feedback revealed by bone conduction microphone in adult zebra finches. Sci. Rep. **5**, 03 (2015)
6. ~~6.~~ Hodgkin, A.L.: The local electric changes associated with repetitive action in a non-medullated axon. J. Physiol. **107**(2), 165–81 (1948) Remove [6] from references
7. Hoppensteadt, F.C., Izhikevich, E.M.: Weakly Connected Neural Networks. Applied Mathematical Sciences. Springer, New York (2012)
8. Kim, S., Park, S.H., Ryu, C.S.: Multistability in coupled oscillator systems with time delay. Phys. Rev. Lett. **79**, 2911–2914 (1997)
9. Kuramoto, Y., Nishikawa, I.: Statistical macrodynamics of large dynamical systems. Case of a phase transition in oscillator communities. J. Stat. Phys. **49**(3), 569–605 (1987)
10. Long, M., Fee, M.: Using temperature to analyse temporal dynamics in the songbird motor pathway. Nature **456**, 189–194 (2008)
11. Mooney, R., Prather, J.: The HVC microcircuit: the synaptic basis for interactions between song motor and vocal plasticity pathways. J. Neurosci. Off. J. Soc. Neurosci. **25**, 1952–1964 (2005)
12. Prescott, S.A.: Excitability: Types I, II, and III, pp. 1–7. Springer New York, New York, NY (2013)
13. Reddy, D., Sen, A., Johnston, G.: Time delay induced death in coupled limit cycle oscillators. Phys. Rev. Lett. **80** (1998)
14. Ramana Reddy, D.V., Sen, A., Johnston, G.L.: Time delay effects on coupled limit cycle oscillators at hopf bifurcation. Phys. D Nonlinear Phenom. **129**(1), 15–34 (1999)
15. Ramana Reddy, D.V., Sen, A., Johnston, G.L.: Dynamics of a limit cycle oscillator under time delayed linear and nonlinear feedbacks. Phys. D Nonlinear Phenom. **144**(3), 335–357 (2000)
16. Schuster, H.G., Wagner, P.: A model for neuronal oscillations in the visual cortex. Biol. Cybern. **64**(1), 77–82 (1990)
17. Strogatz, S.H.: Nonlinear Dynamics and Chaos: With Applications to Physics, Biology, Chemistry and Engineering. Westview Press (2000)
18. Suthers, R.A., Margoliash, D.: Motor control of birdsong. Curr. Opin. Neurobiol. **12**(6), 684–690 (2002)
19. Wilson, H., Cowan, J.: A mathematical theory of the functional dynamics of cortical and thalamic nervous tissue. Kybernetik **13**, 55–80 (1973)
20. Winfree, A.T.: The Geometry of Biological Time. Interdisciplinary Applied Mathematics. Springer, New York (2001)
21. Wittenbach, J.D., Bouchard, K.E., Brainard, M.S., Jin, D.Z.: An adapting auditory-motor feedback loop can contribute to generating vocal repetition. PLOS Comput. Biol. **11**(10), 1–29 (2015)
22. Zeigler, H.P., Marler, P.: Neuroscience of Birdsong. Cambridge University Press (2008)

Author Queries

Chapter 1

Query Refs.	Details Required	Author's response
AQ1	Kindly check and verify that the author name(s) and the identification of the corresponding author(s) are correctly recognized and presented in the correct sequence order and spellings, i.e., given name, middle name/initial, and family name for the authors. In addition, please verify that the E-mail addresses and Affiliation(s) of the corresponding author(s) and co-author(s) shown on the metadata page are valid, and make any necessary amendments if required.	
AQ2	References [6, 12] are given in list but not cited in text. Please cite in text or delete them from list.	

Alternative Texts for Your Images, Please Check and Correct them if Required

Page no	Fig/Photo	Thumbnail	Alt-text Description
6	Fig1	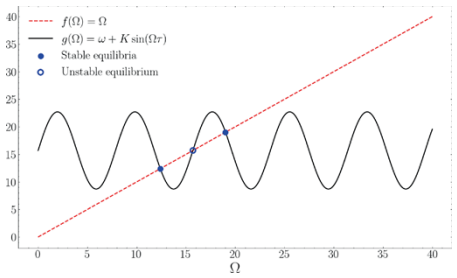	Graph showing two functions: \(f(\Omega) = \Omega \) as a red dashed line and \(g(\Omega) = \omega + K \sin(\Omega \tau) \) as a black wavy line. The x-axis is labeled \(\Omega\) and the y-axis ranges from 0 to 40. Blue dots indicate stable equilibria, and blue circles indicate unstable equilibrium.
8	Fig2	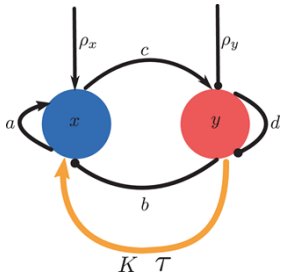	Flow chart depicting a system with two nodes labeled "x" and "y." Node "x" is blue, and node "y" is red. Arrows indicate interactions: "a" loops back to "x," "b" connects "x" to "y," "c" connects "y" to "x," and "d" loops back to "y." Additional arrows labeled "ρ_x" and "ρ_y" point into nodes "x" and "y," respectively. An orange arrow labeled "Kτ" loops from "y" back to "x."
10	Fig3	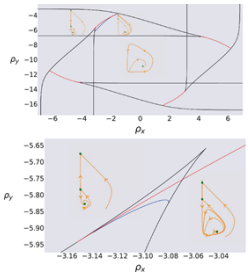	X-Y chart displaying two panels with plots of \(\rho_x\) on the x-axis and \(\rho_y\) on the y-axis. The top panel shows multiple curves in black, red, and blue, with orange arrows indicating direction and small insets of spiral patterns. The bottom panel is a zoomed-in view of a section from the top panel, highlighting detailed interactions between the curves and additional spiral patterns. Key features include intersections and directional flow, emphasizing dynamic relationships between \(\rho_x\) and \(\rho_y\).

Page no	Fig/Photo	Thumbnail	Alt-text Description
11	Fig4	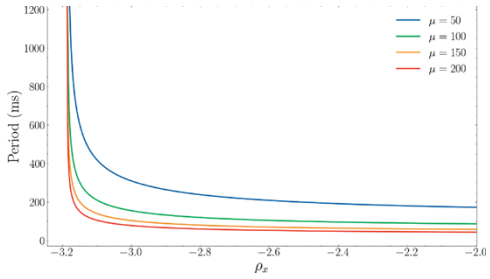	Chart showing the relationship between period (ms) and \(\rho_x \) with four curves representing different \(\mu \) values: 50 (blue), 100 (green), 150 (orange), and 200 (red). The period decreases as \(\rho_x \) increases from -3.2 to -2.0.
13	Fig5	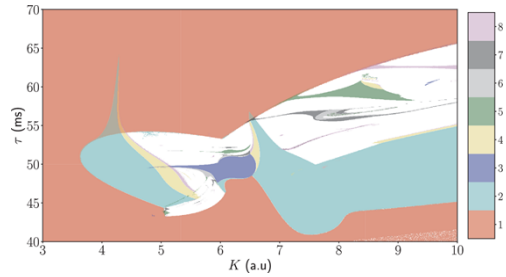	Contour map showing variations in color representing different data regions across a plane. The x-axis is labeled "K (a.u.)" ranging from 3 to 10, and the y-axis is labeled "τ (ms)" ranging from 40 to 70. The map includes a color legend on the right with multiple colors, each indicating a specific data range. The background is predominantly red with areas of green, blue, and other colors, illustrating distinct data zones.